Proceedings of the ASME 2012 International Mechanical Engineering Congress & Exposition
IMECE 2012
November 9-15, 2012, Houston, Texas, United States

IMECE2012-93093

MULTI-LAYER, PSEUDO 3D THERMAL TOPOLOGY OPTIMIZATION OF HEAT SINKS

Caroline McConnell*
Department of Engineering
Union University
Jackson, Tennessee 38305
Email: caroline.mcconnell@my.uu.edu

Georg Pingen
Department of Engineering
Union University
Jackson, Tennessee 38305
Email: gpingen@uu.edu

ABSTRACT

In order to overcome the high computational costs of 3D fluid-thermal topology optimization we introduce a pseudo 3D model consisting of a conductive base-layer and a coupled fluid-thermal design layer. While developed with heat sink designs in mind, the resulting topology optimization approach can be applied to other fluid-thermal design problems where 2D flow effects dominate. We introduce the coupled fluid-thermal solver based on the lattice Boltzmann method, develop and validate the sensitivity analysis for the model, and illustrate the resulting optimization framework for a heat sink design problem.

INTRODUCTION

In component and system cooling applications the design of flow channels and surfaces to promote maximum heat transfer is of great importance. In recent years, particular focus has been placed on the utilization of micro-scale heat transfer effects, leading to multi-scale and multi-physical design problems that are often nonlinear and non-intuitive. To enhance the solution process for such coupled thermo-fluidic design problems, the authors introduce a multi-layer, pseudo 3D thermal topology optimization algorithm. While the specific focus of this work is on the optimal design of heat sinks, the resulting framework is a generic topology optimization framework that can be applied to a wide variety of coupled thermo-fluidic design problems.

Microchannel heat sink optimization is of considerable interest for a wide variety of applications. For example, Liu and Garimella [1] consider analytical models with closed form solutions, Chen et al. [2] consider the optimal design of strip-fin heat sinks, and Balagangadhar and Roy [3] use computational shape optimization to optimize fin and duct designs for coupled fluid-thermal applications, requiring close-to-optimal initial designs as illustrated in Figure 1b. In recent years, increased focus has been placed on topology optimization, which does not require close-to-optimal initial designs and can generate new design features as shown in Figure 1c. Starting with the pioneering work of Borrvall and Petersson [4], gradient-based flow topology optimization approaches have been developed using both Navier-Stokes (e.g. [5, 6]) and kinetic theory based flow solvers [7], and have found application in commercial software packages such as COMSOL Multiphysics. These flow topology optimization

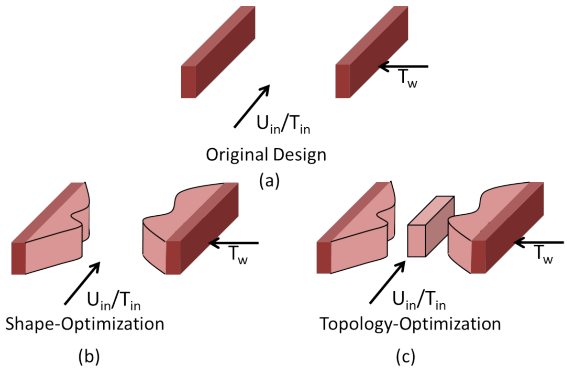

FIGURE 1. Shape vs. Topology Optimization

*Address all correspondence to this author.

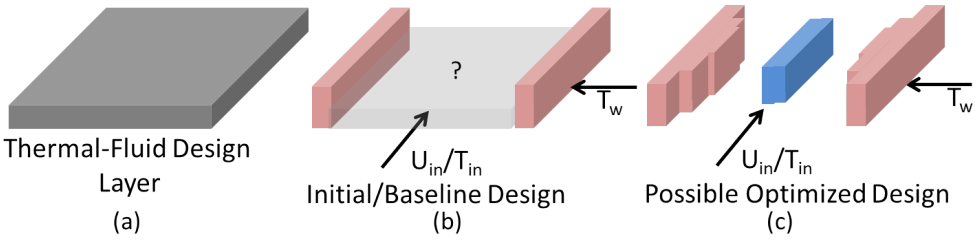

FIGURE 2. Illustration of a 2D thermal optimization, not permitting heated fins surrounded by fluid.

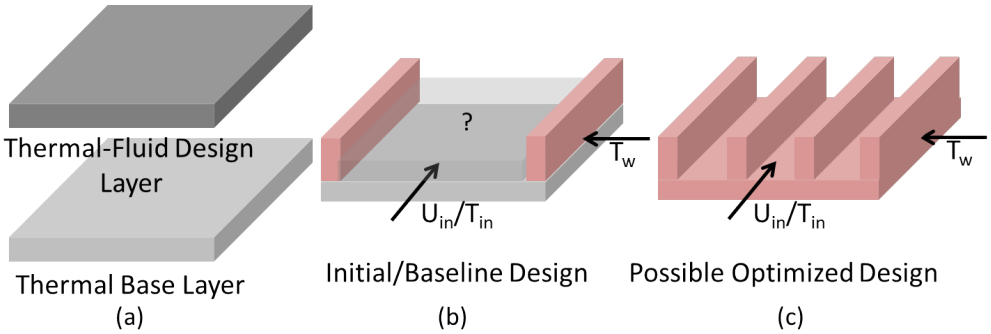

FIGURE 3. Illustration of a pseudo-3D thermal optimization with a conductive base-layer and a design layer allowing for both heat and mass transport.

methodologies have been developed for pure fluid flows and extended to various multi-physical flow phenomena, including 2D coupled heat and mass transfer problems (e.g. [8–11]). While these approaches have shown great promise and an extension of the basic concept from 2D to 3D is straightforward, the computational cost can quickly become prohibitive as shown by Dede [12, 13] who use a 'flattened' thin 3D structure in their recent 3D thermal fluidic topology optimization work. On the other hand, 3D effects are essential for many heat transfer applications and cannot be neglected as illustrated in Figure 2 which shows that 2D optimizations do not permit the generation of heated fins surrounded by a fluid as they are 'free-floating' and disconnected from the remaining structures. To permit the solution of a subset of 3D thermo-fluidic topology optimization problems at close to 2D computational cost, we introduce the use of a thermal base layer that models 3-dimensional conduction effects as illustrated in Figure 3. Thus, while the fluid flow is treated as a 2D problem, heat transfer can occur in 3 dimensions, permitting topology optimization of e.g. lab-on-a-chip devices.

In the following sections, we will first introduce the overall design problem and problem formulation, followed by an analytical motivation, a discussion of the lattice Boltzmann flow solver, and a derivation and validation of the corresponding analytical sensitivity analysis. We will illustrate the topology optimization approach by presenting preliminary results for the optimal design of a heat sink using: a) general topology optimization, b) the optimization of a single and triple fin, and c) the optimization of a multi-fin heat sink. As part of this work, we will show that the nonlinear interactions between thermal and fluidic effects lead to poor convergence behavior of the optimizer with a preference for undesired intermediate design variables. By employing different functional dependencies between the design variables and fluid/thermal properties as well as utilizing penalty formulations, we begin to explore options to improve the desired convergence of the optimization algorithm to final designs consisting of pure fluid and pure solid material.

DESIGN PROBLEM FORMULATION

The goal of the present work is the development of a topology optimization algorithm for heat sink optimizations as illustrated in Figure 3b. Having a heated wall, thermal base-layer permitting conduction, and a fluid-thermal design layer, we want to determine the geometry of a design that promotes the maximum heat transfer from the heated walls. We can formulate the following generic unconstrained topology optimization problem:

$$\begin{aligned} &\min_{\mathbf{s}} \mathscr{F}(\mathbf{s}, f(\mathbf{s}), g(\mathbf{s})), \\ &\text{s.t. } \{ f, g, \quad \text{solves the governing equations for a given } \mathbf{s}, \end{aligned} \tag{1}$$

where $\mathscr{F}$ is a particular performance (objective) functional (negative heat transfer in this case), f and g are the respective corre-

sponding state variables for mass and heat transfer, and **s** is the vector of design variables. To solve for the mass and heat transfer state variables, we utilize the lattice Boltzmann method as discussed later. The thermal and hydrodynamic lattice Boltzmann equations are then augmented to enable a continuous transition from fluid to solid as needed for gradient-based topology optimization. The resulting thermal optimization problem presented in equation (1) is solved with a gradient-based optimization algorithm, the Globally Convergent Method of Moving Asymptotes (GCMMA) presented by Svanberg [14].

In order to reduce computational cost, the resulting analysis and optimization framework will not be fully-3D, but instead consist of a thermally conductive base-layer and thermo-fluidic design layer as illustrated in Figure 3. This approach is motivated by the common use of layer-deposition techniques in the fabrication of micro-fluidic devices and has been used by Kreissl et al. [15] for the optimal design of flexible micro-fluidic devices. This approximation will be most accurate when the flow features are relatively high compared to the flow-channel width, such that the fluid flow is accurately represented by the 2D model.

Analytical Solution for Optimal Number of Fins

In order to show that one would indeed expect the formation of fins for the design problem shown in Figure 3b under typical flow conditions, a brief analytical analysis is performed. The thermal energy balance for fluid flowing between heated walls is given as:

$$Q = n_f h A \Delta T_{lm} = \dot{m} c \Delta T_m, \tag{2}$$

where Q is the heat flux, n_f is the number of flow channels, h is the convection coefficient, A is the surface area, ΔT_{lm} is the log-mean temperature difference ($\Delta T_{lm} = \frac{\Delta T_e - \Delta T_i}{ln(\Delta T_e / \Delta T_i)}$, where $\Delta T_e = T_s - T_e$ and $\Delta T_i = T_s - T_i$ with e, s, and i denoting exit, surface, and inlet respectively), $\dot{m}$ is the mass flowrate, c is the specific heat, and $\Delta T_m = T_e - T_i$ is the mean temperature difference of the fluid.

We can now utilize the illustration in Figure 4 for constant temperature fins with fully developed laminar flow to analytically determine a relation for the optimum number of fins needed to achieve maximum heat transfer. Considering the solution for flow between parallel plates, a relation for the average channel velocity V_{avg} can be found for a given pressure drop $\Delta P = P_2 - P_1$ as:

$$V_{avg} = \frac{\Delta P w^2}{12 \mu L}, \tag{3}$$

where w is the individual channel width defined by the ratio of overall width W to the number of flow channels n_f ($w = \frac{W}{n_f}$), μ

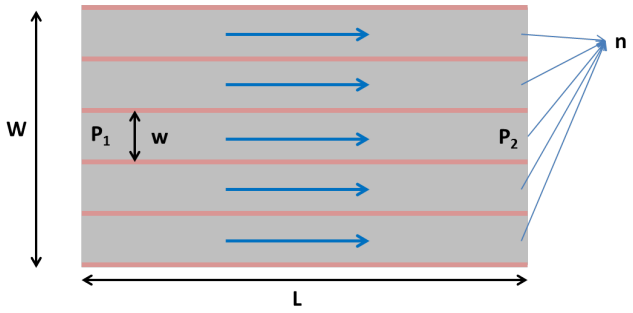

FIGURE 4. Notation for Analytical Fin Optimization

is the dynamic viscosity, and L is the channel length. The mass flowrate can then be determined as:

$$\dot{m} = \rho V_{avg} A = \rho V_{avg} W H = \frac{\Delta P W^3 H}{12 n_f^2 \nu L}, \tag{4}$$

where ρ is the fluid density, H is the height of the channels, and ν is the kinematic viscosity. We can now use these relations to express the right side of Eq. 2 in terms of the number of flow channels n_f, fluid temperatures, and known geometrical and fluid properties. The left side of Eq. 2 can be modified through the use of the Nusselt number. For fully developed laminar flow through channels with constant surface temperatures and an infinite height to width ratio inherent to our pseudo 3D model, a Nusselt number of $Nu = 7.54 = \frac{hD_h}{k}$ is commonly given in literature [16], where h is the convection coefficient, $D_h = 2\frac{W}{n_f}$ is the hydraulic diameter, and k is the conduction coefficient of the fluid. Further, replacing the surface area of the channel with $A = 2 n_f L H$ leads to the following heat flux balance with the only unknowns being the number of flow channels n_f and the fluid exit temperature T_e:

$$Q = \frac{n_f^2 Nuk L H \Delta T_{lm}}{2W} = \frac{\Delta P W^3 H c \Delta T_m}{12 n_f^2 \nu L}. \tag{5}$$

Solving this equation for the fluid exit temperature T_e and plugging back in leads to the following relation for the overall heat flux as a function of the number of flow channels n_f:

$$Q = \frac{\Delta P W^3 H c}{12 n_f^2 \nu L} \left[T_s - (T_s - T_i) e^{-\frac{6 Nu \alpha L^2 \mu n_f^4}{\Delta P W^4}} - T_i \right], \tag{6}$$

where α is the thermal diffusivity ($\alpha = \frac{k}{\rho c}$). We can now determine the optimal number of fins by setting $\frac{dQ}{dn_f} = 0$ and solving

for n_f. Alternatively we can plot Eq. 6 as done for typical lattice Boltzmann fluid and geometry values in Figure 5, which shows that having approximately 6 flow channels represents the optimal fin/channel configuration for a particular choice of parameters. At this point, it should be pointed out that the thickness of the fins was neglected during the present analytical analysis and would lead to a decrease in the optimal number of flow channels. However, the presented analytical derivation shows that there is a specific number of fins that lead to optimum heat transfer. It is this realization that motivates the development of a generalized topology optimization algorithm for heat sink design.

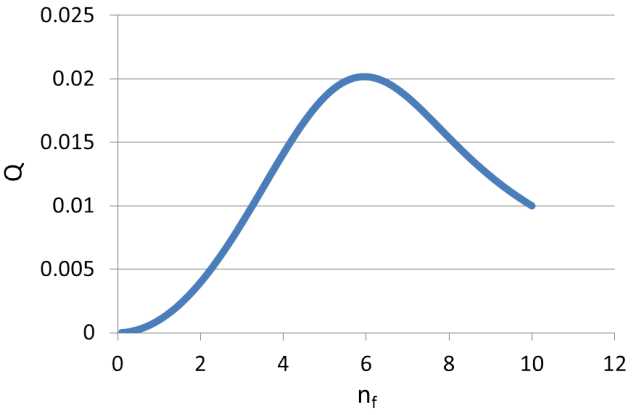

FIGURE 5. Relation between number of flow channels n_f and heat flux Q in Watts.

Thermal Lattice Boltzmann Method

Since its introduction, the Lattice Boltzmann method (LBM) has become a viable alternative to Navier-Stokes based methods for many flow scenarios [17, 18]. For coupled thermo-fluidic problems three main methods - the two distribution approach, the hybrid passive-scalar approach, and the multiple-relaxation-time single distribution approach - have been developed and applied to a variety of problems including forced and natural convection (e.g. [19, 20]). In the present work we use the two distribution approach due to its simplicity and ability to represent varying Prandtl numbers.

The two distribution function thermal LBM as used in this work closely follows the models presented by Kao et al. [21] and Yan and Zu [20] except for the use of three dimensional thermal distribution functions. The thermal hydrodynamic lattice Boltzmann method approximates the Navier-Stokes and energy equations and results in a two-step computational process for fluidic f and thermal components g. The key difference between the fluid and thermal distribution functions is the definition of the equilibrium distribution function as illustrated in the following equations:

$$\textit{Collision} - \mathbf{C}:$$

$$\widetilde{f_\alpha}(\mathbf{x}_i,t) = f_\alpha(\mathbf{x}_i,t) - \frac{1}{\tau_f}[f_\alpha(\mathbf{x}_i,t) - f_\alpha^{eq}(\mathbf{x}_i,t)], \tag{7}$$

$$\widetilde{g_\alpha}(\mathbf{x}_i,t) = g_\alpha(\mathbf{x}_i,t) - \frac{1}{\tau_t}[g_\alpha(\mathbf{x}_i,t) - g_\alpha^{eq}(\mathbf{x}_i,t)], \tag{8}$$

$$\textit{Propagation} - \mathbf{P}:$$

$$f_\alpha(\mathbf{x}_i + \delta t\mathbf{e}_\alpha, t+\delta t) = \widetilde{f_\alpha}(\mathbf{x}_i,t), \tag{9}$$

$$g_\alpha(\mathbf{x}_i + \delta t\mathbf{e}_\alpha, t+\delta t) = \widetilde{g_\alpha}(\mathbf{x}_i,t). \tag{10}$$

The fluid and thermal equilibrium distribution functions are given respectively as:

$$f_\alpha^{eq} = w_{\alpha,f}\rho\left[1 + 3(\mathbf{e}_\alpha\cdot\mathbf{u}) + \frac{9}{2}(\mathbf{e}_\alpha\cdot\mathbf{u})^2 - \frac{3}{2}\mathbf{u}^2\right], \tag{11}$$

$$g_\alpha^{eq} = w_{\alpha,T}\mathbf{T}\left[1 + 3(\mathbf{e}_\alpha\cdot\mathbf{u})\right], \tag{12}$$

where ρ is the macroscopic density, $\mathbf{T}$ is the macroscopic temperature, $\mathbf{u}$ is the macroscopic velocity, and w_α are lattice weights that depend on the lattice geometry. The lattice geometry differs for the velocity and thermal distributions. The velocity distribution is defined by a two dimensional, nine velocity (D2Q9) model (see Figure 6a), allowing for the recovery of the macroscopic density, velocity and pressure. The thermal distribution is defined as a three dimensional, 7 velocity (D3Q7) model [22] (see Figure 6b), allowing for the heat transfer from the thermal base layer to the design layer and the determination of the macroscopic temperature values. Due to the difference in lattice geometry the weights for the velocity distribution are $w_{\alpha,f} = [\frac{4}{9}, \frac{1}{9}, \frac{1}{9}, \frac{1}{9}, \frac{1}{9}, \frac{1}{36}, \frac{1}{36}, \frac{1}{36}, \frac{1}{36}]$ and the weights for the thermal distribution are $w_{\alpha,T} = [\frac{1}{4}, \frac{1}{8}, \frac{1}{8}, \frac{1}{8}, \frac{1}{8}, \frac{1}{8}, \frac{1}{8}]$.

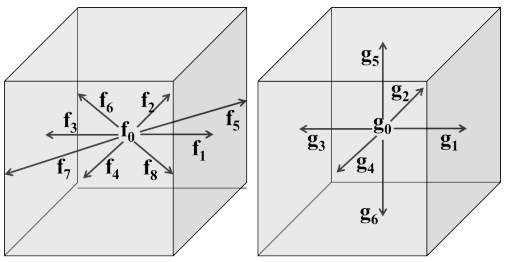

a) D2Q9 b) D3Q7

FIGURE 6. Directions for D2Q9 and D3Q7 LBM lattices.

Viscosity (ν) and thermal diffusivity (α) can be shown to be related to their respective relaxation times τ_g and τ_f by a

Chapman-Enskog expansion of the Lattice Boltzmann equations [23, 24]. The relationships are given by

$$\nu = (\tau_f - 1/2)c_s^2 \delta t \tag{13}$$
$$\alpha = (\tau_g - 1/2)c_s^2 \delta t. \tag{14}$$

For a given fluid, ν and α are related by the dimensionless Prandtl number

$$Pr = \frac{\nu}{\alpha}. \tag{15}$$

In order to continuously transition from fluid to solid and vice-versa as required for gradient-based topology optimization, the following physical properties/variables must vary as a function of the mapped design variables $p(x) = p(s(x))$: velocity, thermal diffusivity and base-layer to design-layer conductivity. Here it should be noted that the ultimate goal is not the accurate representation of intermediate material as the final design should consist primarily of pure fluid and pure solid material. Pingen et al [7] have shown that the porosity model of Spaid and Phelan [25] can be used to continuously scale the velocity of the fluid:

$$\tilde{\mathbf{u}}(t,\mathbf{x}) = (1 - \mathbf{p}(\mathbf{x})^{\kappa_v})\, \mathbf{u}(t,\mathbf{x}), \tag{16}$$

where $\mathbf{p}(\mathbf{x})$ is substituted into the equilibrium distribution functions (11) and (12) instead of $\mathbf{u}$ and a shaping factor of $\kappa_v = 3$ has been introduced in order to improve the convergence properties of the design optimization process.

Pingen and Meyer [8] have introduced a similar scaling to transition from the thermal diffusivity of a fluid α_f to that of a solid α_s using the shaping factor κ_T:

$$\tilde{\alpha}(t,\mathbf{x}) = \alpha_f + (\alpha_s - \alpha_f)\mathbf{p}(\mathbf{x})^{\kappa_T}. \tag{17}$$

Finally, in order to transition from an insulated (fluid) to a conductive (solid) boundary between the base-layer and design-layer, a partial bounce-back boundary condition - analogous to the work by Pingen et al [26] for fluids - is applied to the thermal distribution function in place of the propagation step:

$$\tilde{g}_5^2(t,\mathbf{x}) = g_6^2(1 - \mathbf{p}(\mathbf{x})^{\kappa_p}) + g_5^1(\mathbf{p}(\mathbf{x}))^{\kappa_p} \tag{18}$$
$$\tilde{g}_6^1(t,\mathbf{x}) = g_5^1(1 - \mathbf{p}(\mathbf{x})^{\kappa_p}) + g_6^2(\mathbf{p}(\mathbf{x}))^{\kappa_p}. \tag{19}$$

Here, the shaping factor is defined by κ_p and the boundary interaction is illustrated in Figure 7 for one time-step. The result

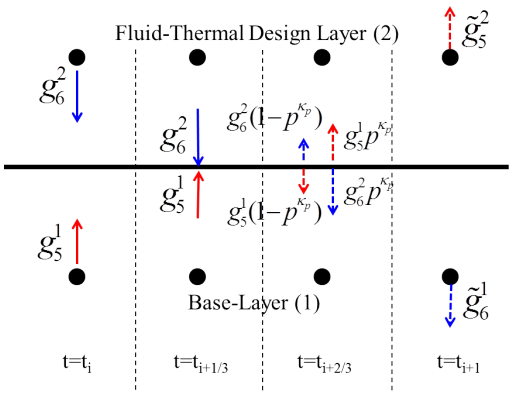

FIGURE 7. Scaling of conductivity between base-layer and design-layer.

is an interface between the layers that transitions from being a 'zero-flux' insulator when $p = 0$ (reflective to thermal fluxes) to permitting full heat flux through the boundary in the case of a solid $p = 1$.

It is important to note that the developed thermal topology optimization framework is currently applied to steady-state flows approximated through the following fixed-point formulation:

$$\mathbf{R}(f,g,\mathbf{p}) = \mathbf{M}(f,g,\mathbf{p}) - \begin{Bmatrix} f \\ g \end{Bmatrix} = \mathbf{0}. \tag{20}$$

Here $\mathbf{R}$ denotes the residual vector and the operator $\mathbf{M}$ performs one collision and propagation step to advance the flow and temperature to the next time step.

Thermal Sensitivity Analysis for Topology Optimization

In order to solve the optimization problem (1) using a gradient-based optimization algorithm, the design sensitivities of the performance functional with respect to the design variables $\frac{d\mathscr{F}}{ds_j}$ are required. Due to the large number of design variables, an adjoint formulation is traditionally used and was derived for hydrodynamic and thermal lattice Boltzmann based topology optimization by Pingen and co-workers [7, 8] as:

$$\frac{d\mathscr{F}}{ds_j} = \frac{\partial \mathscr{F}}{\partial s_j} - \left[J^{-T} \frac{\partial \mathscr{F}}{\partial [\mathbf{f},\mathbf{g}]} \right]^T \frac{\partial \mathbf{R}}{\partial s_j}, \tag{21}$$

where $\mathbf{f}$ and $\mathbf{g}$ are the steady-state fluid and thermal distribution functions approximated through the fixed-point formulation (20) and $\mathbf{J} = \frac{\partial \mathbf{R}}{\partial [\mathbf{f},\mathbf{g}]} = \frac{\partial \mathbf{M}}{\partial [\mathbf{f},\mathbf{g}]} - \mathbf{I}$ is the Jacobian of the fixed-point problem.

The evaluation of the partial derivatives $\frac{\partial \mathscr{F}}{\partial s_j}$, $\frac{\partial \mathscr{F}}{\partial [\mathbf{f},\mathbf{g}]}$, $\frac{\partial \mathbf{R}}{\partial s_j}$, and $\frac{\partial \mathbf{M}}{\partial [\mathbf{f},\mathbf{g}]}$ is necessary to solve the adjoint sensitivity equation (21). The evaluation of these derivatives based on analytically derived expressions is discussed in detail by Pingen and co-workers [7,8] and the derivatives of the residual with respect to the design variables $\partial \mathbf{R}/\partial s_j$ follow a procedure similar to the Jacobian. Thus, the present work specifically focuses on the differences between the analytical 2D thermal LBM Jacobian derived by Pingen and Meyer [8] and the pseudo 3D Jacobian required for the present work. Those differences are due to the use of the D3Q7 thermal model and the thermal interaction between base-layer and design-layer as shown in equation (18).

For the Jacobian, the derivative of the operator $\mathbf{M}$ can be separated into a collision and a propagation step:

$$\left(\frac{\partial \mathbf{M}}{\partial [\mathbf{f},\mathbf{g}]}\right)^T = \left(\frac{\partial \mathbf{P}}{\partial [\mathbf{f},\mathbf{g}]}\right)^T \left(\frac{\partial \mathbf{C}}{\partial [\mathbf{f},\mathbf{g}]}\right)^T. \tag{22}$$

Collision Jacobian: The sensitivities of the collision operator with respect to the distribution functions, $(\partial \mathbf{C}/\partial [\mathbf{f},\mathbf{g}])^T$ are determined by differentiating the fluid and thermal collision steps (7) and (8) leading to the following localized collision step Jacobian at each lattice node:

$$\frac{\partial \mathbf{C}}{\partial [\mathbf{f},\mathbf{g}]} = \frac{\partial [\widetilde{f},\widetilde{g}]_\alpha}{\partial [f,g]_\beta} = \frac{\partial [f,g]_\alpha}{\partial [f,g]_\beta} - \frac{1}{\tau}\left[\frac{\partial [f,g]_\alpha}{\partial [f,g]_\beta} - \frac{\partial [f,g]^{eq}_\alpha}{\partial [f,g]_\beta}\right]. \tag{23}$$

Here, α and β represent the 9 discretizations of velocity space for the fluid distribution function f and the 7 discretizations of velocity space for the thermal distribution function g. The partial derivatives $\partial f_\alpha/\partial f_\beta = 1$ and $\partial g_\alpha/\partial g_\beta = 1$ when $\alpha = \beta$ and zero otherwise.

Thus, only the derivatives of the equilibrium distribution functions (11) and (12) are non-trivial. As a one-way coupling is present between fluid and thermal state variables (no buoyancy effects are considered), the velocity equilibrium distribution function f^{eq} depends only on the mass transfer variables ρ and $\mathbf{u}$, but the thermal equilibrium distribution function g^{eg} is coupled and depends on both mass and thermal transfer through the variables $\mathbf{u}$ and $\mathbf{T}$. Following the detailed derivation by Pingen and Meyer [8] for 2D problems, this leads to a block diagonal global Jacobian and a highly populated, 16×16 (pseudo 3D), local Jacobian of the collision operation $\mathbf{C}_i$ at each lattice node i shown in Figure 8:

$$\left(\frac{\partial \mathbf{C}_i}{\partial [f_\beta, g_\beta]}\right)^T = \left(\frac{\partial \left[\widetilde{f}_\alpha, \widetilde{g}_\alpha\right]}{\partial [f_\beta, g_\beta]}\right)^T = \begin{pmatrix} \frac{\partial \widetilde{f}_0}{\partial f_0} & \cdots & \frac{\partial \widetilde{g}_6}{\partial f_0} \\ \vdots & \ddots & \vdots \\ \frac{\partial \widetilde{f}_0}{\partial g_6} & \cdots & \frac{\partial \widetilde{g}_6}{\partial g_6} \end{pmatrix} \tag{24}$$

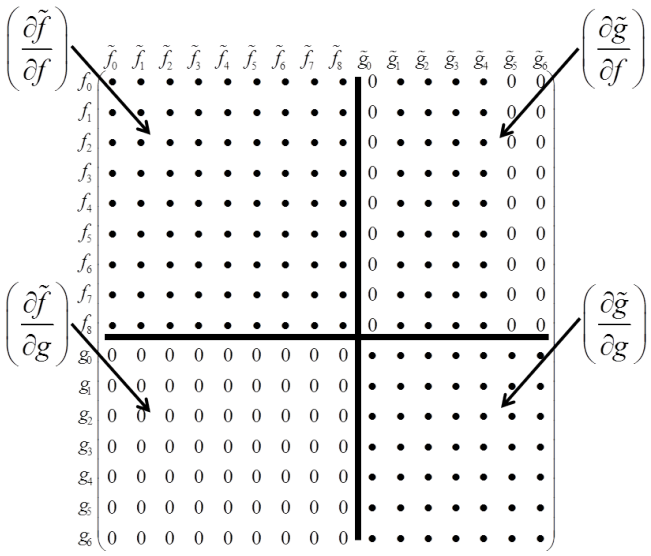

FIGURE 8. Local 16×16 Collision Jacobian

Considering the local collision Jacobian depicted in Figure 8, the 9×9 block in the top left corner represents the hydrodynamic component of the Jacobian $\frac{\partial \widetilde{f}_\alpha}{\partial f_\beta}$ and is fully populated. The 9×7 block in the top right corner represents the coupling between thermal and hydrodynamic distribution functions $\frac{\partial \widetilde{g}_\alpha}{\partial f_\beta}$. As the stationary distribution function g_0 and those moving in the vertical direction (3rd dimension) g_5 and g_6 are independent of the flow velocities, those columns are zero. The 7×9 block in the bottom left corner represents the coupling between hydrodynamic and thermal distribution functions $\frac{\partial \widetilde{f}_\alpha}{\partial g_\beta}$ and is filled with all zeros due to the one-way coupling in the present model. Finally, the 7×7 block in the bottom right corner represents the thermal component of the Jacobian $\frac{\partial \widetilde{g}_\alpha}{\partial g_\beta}$ and is fully populated.

Propagation Jacobian: The second component needed for the determination of the Jacobian of the lattice Boltzmann system is the derivative of the propagation operator with respect to the distribution functions, $(\partial \mathbf{P}/(\partial [\mathbf{f},\mathbf{g}]))^T$. In previous work by Pingen and co-workers [7, 8] this simply led to a shifting of the rows from the collision Jacobian as the basic propagation step leads to a movement of distribution functions to neighboring nodes. In the present model, the partial bounce-back condition (18) modifies the propagation step and leads to the following

augmented propagation Jacobian:

$$\begin{aligned}\frac{\partial \mathbf{P}}{\partial [f,g]_\beta} &= \frac{\partial [f,g]_\alpha (\mathbf{x}_i,t)}{\partial [f,g]_\beta (\mathbf{x}_j,t)} \\ &= \frac{\partial \left[\tilde{f},\tilde{g}\right]_\alpha (\mathbf{x}_i-\delta t\mathbf{e}_\alpha,t-\delta t)}{\partial [f,g]_\beta (\mathbf{x}_j,t)} \\ &= \begin{cases} 1-\mathbf{p}(\mathbf{x}^{\kappa_p}) & \text{if g, } \beta=[5,6],\ \alpha=[6,5],\ \mathbf{x}_j=\mathbf{x}_i, \\ \mathbf{p}(\mathbf{x})^{\kappa_p} & \text{if g, } \beta=\alpha=[5,6],\ \mathbf{x}_j=\mathbf{x}_i-\delta t e_\alpha, \\ 1 & \text{if } \beta=\alpha,\ \mathbf{x}_j=\mathbf{x}_i-\delta t\mathbf{e}_\alpha, \\ 0 & \text{otherwise.} \end{cases}\end{aligned} \tag{25}$$

From this equation it can be seen that when the Jacobians of the collision and propagation operators are combined, the Jacobian of the propagation operator primarily leads to a shifting of rows from the collision Jacobian except for the vertical components of the thermal distribution function (g_5, g_6), which lead to a scaling and addition of the corresponding rows from the collision Jacobian.

Objective Function: The objective for the example problems presented in this work is to minimize the negative net heat flux out of the design domain measured between the 2nd and 3rd node at the inlet and the 3rd to last and 2nd to last nodes along the outlet. Nodes at least 1 removed from the inlet/outlet where chosen to reduce boundary effects, leading to the following performance functional:

$$\begin{aligned}\mathscr{F} &= -\Delta\mathscr{H}\mathscr{F}_{net} = -(\mathscr{H}\mathscr{F}_{out} - \mathscr{H}\mathscr{F}_{in}) \\ &= \int_{x=2} g_1 - \int_{x=3} g_3 - \int_{x=lx-2} g_1 + \int_{x=lx-1} g_3.\end{aligned} \tag{26}$$

Sensitivity Validation: In order to ensure that the analytical sensitivity analysis is accurate, a finite difference sensitivity analysis was implemented. The finite difference verification was performed by finding the heat flux from the domain with a single, intermediate design variable fin ($s = 0.5$). The design variable was then perturbed by a factor ε, leading to a change in the corresponding heat flux. The difference between the two heat flux values was divided by the perturbation ε and then compared to the analytic sensitivity value in order to compute the percent difference between both. For a small interval around the design variable $s = 0.5$ the sensitivities are expected to behave in a nearly linear manner resulting in good agreement between analytical and finite-difference results. It can be seen from Figure 9 that for epsilon values from $10^{-7} - 10^{-3}$ the analytical and finite-difference sensitivities are in good agreement and the implemented analytical sensitivity analysis is accurate. For smaller ε values the finite difference results are inaccurate due to numerical noise and for larger ε values the linear finite difference approximation inaccurately approximates the underlying nonlinear problem.

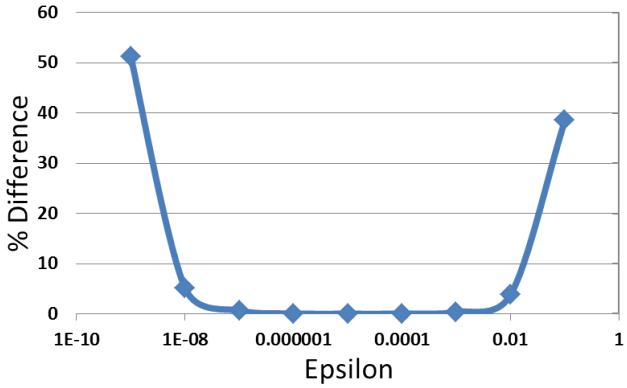

FIGURE 9. Comparison of Analytical and Finite Difference Sensitivities

EXAMPLES

The goal of this work is the development of a topology optimization framework to determine optimal heat-sink designs. The objective is to maximize the heat transfer from the thermal base-layer of the design problem illustrated in Figure 10. The blue color in the figure represents a prescribed fluid region at the front and back of the design domain in order to avoid inlet and outlet effects. Similarly, the sides are prescribed as solid material. The temperature of the fluid at the inlet is set to 20 degrees in LBM units and the thermal base-layer side temperature is set to 200 degrees in LBM units. The solid material is highly conductive, as to model material commonly used in heat sinks, the thermal diffusivity in this problem is $\alpha_s = 0.5$ in LBM units. The fluid is much less conductive, having a thermal diffusivity set to $\alpha_f = 0.00211$ in LBM units. The scaling factors of this problem are set to $\kappa_p = 3$, $\kappa_v = 3$, and $\kappa_t = 3$. The problem is solved on a 40×40 mesh with a design domain of 22×38 where each lattice node is linked to one design variable leading to 836 total design variables.

With these settings, the optimal design in Figure 11 was obtained. The dark blue at the bottom of the spectrum of the porosity scale in Figure 11 represents complete fluid, the dark red at the top of the same scale represents complete solid. The results show a large amount of intermediate porosities throughout the design domain, resulting in a non-intuitive, impractical and non-physical design. While the intermediate porosities might suggest a very fine fin structure smaller than permitted by the problem resolution, the ultimately desired result is a design with no intermediate porosities in order to produce a realistic heat sink design.

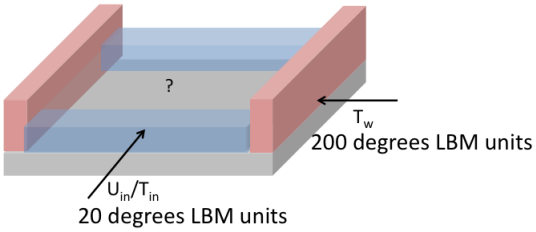

FIGURE 10. Initial Design Domain

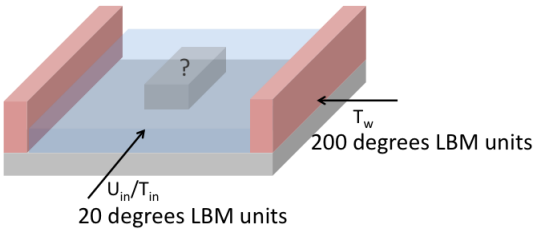

FIGURE 12. Single Fin Design Domain

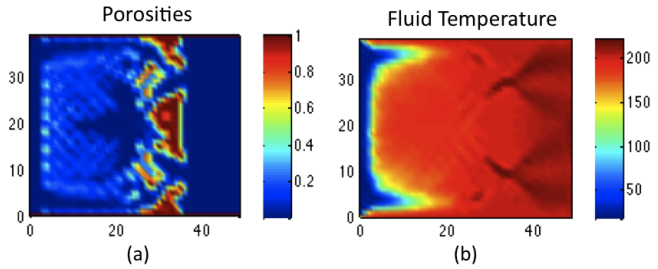

FIGURE 11. Optimization of Initial Design Domain on a 40×40 Mesh

Due to this undesired design outcome we simplify our design setup in the following section in order to further investigate the behavior of the optimization algorithm.

Single and Triple Fin Experiments

Instead of a design domain with design variables corresponding to each lattice node, we simplify the problem to the creation of one fin in the center of the domain as shown in Figure 12. The area around the fin is prescribed fluid and the fin is only allowed to change as one design variable. With this new design domain we keep all remaining variables unchanged.

Using this design domain the results shown in Figure 13 are obtained. The fin converges towards a pure solid but stops at a result of $s = 0.9025$ instead of becoming completely solid. Having a fin with this porosity improves the objective value from that of an empty design domain. With a completely fluid design domain the objective value of the system is -7.8 and the objective value with a fin of porosity $s = 0.9025$ is -15.2. The design stopped short of forming a solid fin because the objective for $s = 0.9025$ is better than that of a completely solid fin as shown in Figure 14. This effect is due to the relative interplay of fluidic and thermal effects as the design variable changes from fluid to solid and can possibly be overcome through the use of different scaling factors κ.

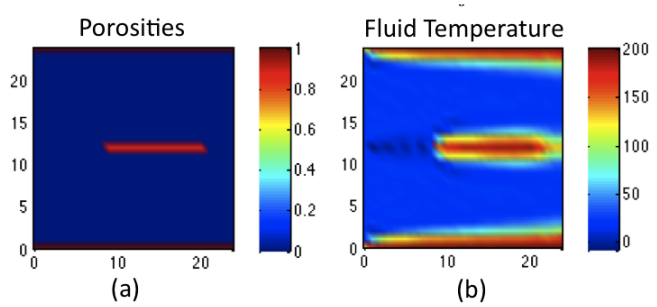

FIGURE 13. Single Design Variable Fin on a 25×25 Mesh

To create an end result of complete fluid or solid features the porosity vs heat flux graph must be continuously decreasing. Figure 14 shows that objective values at the current design settings dip lower than the objective value for a complete solid. Options to improve this functional behavior are investigated next.

Kappa and Penalty Testing

First we investigate possible changes to the scaling factors κ_v, κ_t, and κ_p to change the functional dependency of the hydrodynamic and thermal parameters on the design variables. As we are primarily concerned with designs that consist of complete fluid and solid without intermediate porosities, these functional relations can be selected in order to obtain a better behaving optimization problem. The scaling factor kappa allows a change in values for κ_v, κ_t, and κ_p, without impacting the accuracy of the analysis for the final converged design.

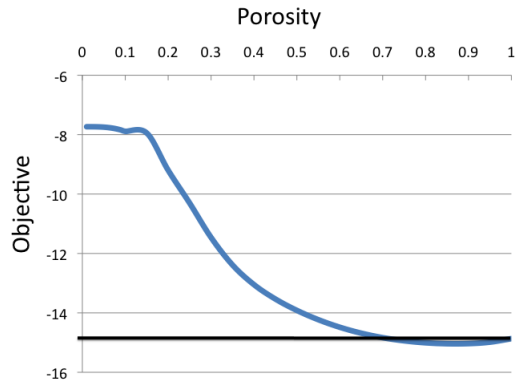

FIGURE 14. Objective vs. Porosity With All Kappas Equal to 3 for a Single Design Variable Fin on a 25×25 Mesh

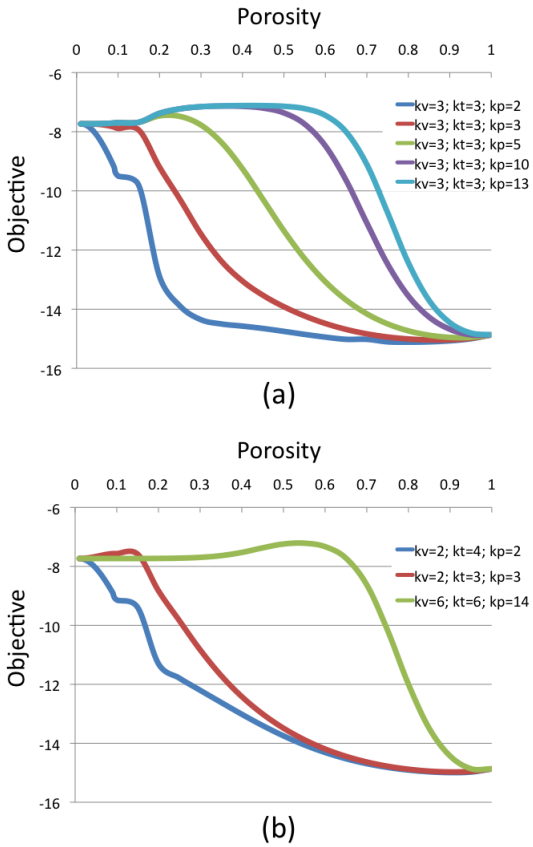

FIGURE 15. Kappa Testing (a) Objective vs. Porosity With κ_p Changing (b) Objective vs. Porosity With Different κ_v, κ_t, and κ_p Values

A sample of the different testing results is shown in Figure 15a and b for different kappa values. Based on the results shown in Figure 15a, increasing κ_p solved the problem of objective values dipping lower than those with a porosity of one but created an increase in the objective at low porosities. Since combinations of different kappas are not producing the desired continuously decreasing result we turn to a penalty formulation. Penalty approaches are commonly used in structural topology optimization and are referred to as SIMP-models (Solid Isotropic Material with Penalization) [27]. For our problem we augment the objective through the following penalty formulation:

$$\mathscr{F}_P = \mathscr{F} + C(p^f)(1-p^f), \tag{27}$$

where C and f are scaling parameters that can be adjusted to improve the behavior of the optimization problem for intermediate porosities by penalizing those intermediate values. Using the kappa results shown in Figure 15 we can apply this penalty formulation to see if there is a penalty factor that works for our design problem. Using the present problem with $\kappa_v = 2$, $\kappa_t = 4$, $\kappa_p = 2$, and a penalty factor with $C = 2$ and $f = 2$ leads to a continuously decreasing relation between the design variable and objective as shown in Figure 16. Applying this result to one design variable fins in the middle of the design domain works for the 25×25 mesh as shown in Figure 17, leading to a completely converged design.

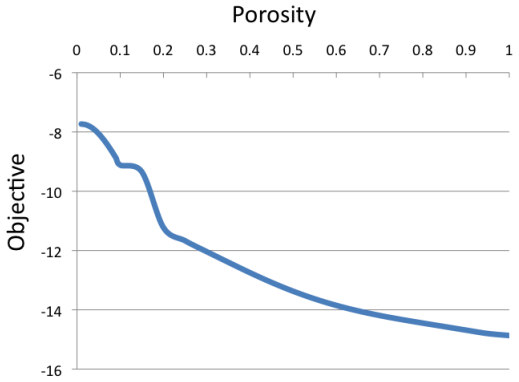

FIGURE 16. Objective vs. Porosity With Penalty Factor Correction

We now want to increase the complexity of the design problem by re-introducing additional design variables. To do so, we solve a design problem with 3 design variables for the possible generation of three fins. The results for this study are shown in Figure 18 and confirm that the use of $\kappa_v = 2$, $\kappa_t = 4$, $\kappa_p = 2$, and

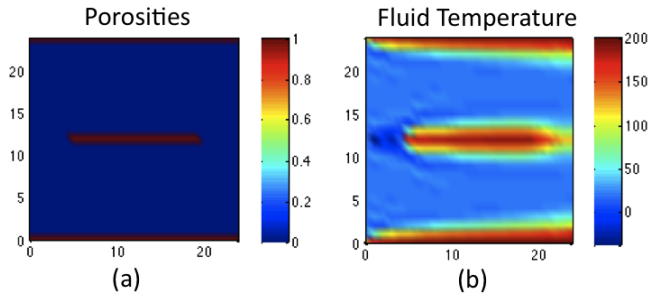

FIGURE 17. Optimization of One Fin With Penalty Factor for a 25×25 Mesh

a penalty factor with C=2 and f=2 leads to converged optimal designs for the current problem set-up.

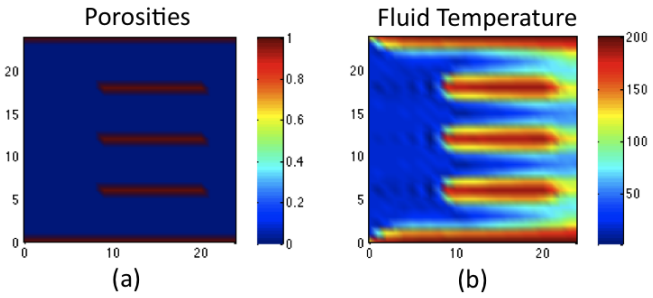

FIGURE 18. Optimization for Three Fins With Penalty Factor for a 25×25 Mesh

Optimization With Seven Fins

As shown in the analytical section of this paper, there is an optimal number of fins for a given design domain. Having tested a single and triple fin design with one and three design variables, respectively, we now want to investigate a problem with 7 design variables and therefore a possibility of generating 7 fins in the domain as shown in Figure 19. The goal is to determine if the optimizer can find the optimal configuration of fins. In order to account for the fact that 7 design variables are now penalized, the scaling factor C has been adjusted to a value of $C = 1.30$ to facilitate converged designs while all other settings are maintained from the previous problems.

As shown in Figure 20, our optimization framework leads to a design with three fins, equivalent to that shown in Figure 18. Given the design space of seven design variables, this 3 fin solution is indeed optimal. Of interest is also to see how the optimizer progresses towards the design, which is shown in Figure

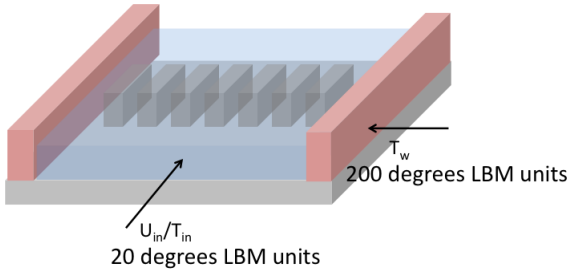

FIGURE 19. Initial Design Domain For Seven Fins

20. First the optimizer begins to form 7 fins as shown in Figure 20b. Then the optimizer reduces the number of fins to 3 in Figure 20c which become completely solid at different rates. The progression of the objective as a function of design iterations is shown in Figure 20a. This example problem shows the potential of the developed thermal topology optimization approach. More work is needed to develop a general penalty approach that is applicable to the general topology optimization problem where each lattice node is linked to one design variable as was the case in the first example problem shown in Figure 11.

CONCLUSION

We have introduced a lattice Boltzmann method based pseudo 3D fluid-thermal topology optimization approach and have developed the corresponding adjoint sensitivity analysis. We have validated the sensitivity analysis and have applied the resulting optimization framework to the optimal design of a heat sink. Differing from past LBM based topology optimization, it was shown that the non-linear nature and complex interaction of hydrodynamic and thermal effects necessitates the use of a penalty formulation in order to prevent intermediate porosities. The resulting optimization framework was than illustrated for a multi-fin heat sink optimization. Future work will focus on generalizing the penalty formulation such that it is applicable to the more general topology optimization problem where each fluid node corresponds to a design variable, maximizing the design space and thus permitting the generation of a wider range of optimal designs.

ACKNOWLEDGMENT

The authors would like to acknowledge support by Union University through an Undergraduate Research Grant in support of the presented work.

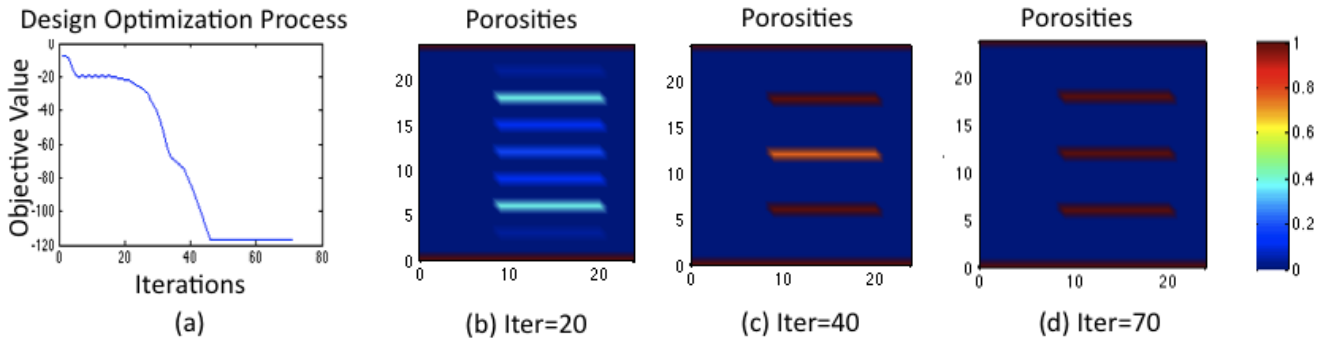

FIGURE 20. Iterations of Seven Fins: (a) Optimization vs. Iterations (b) System After 20 Iterations (c) System after 40 Iterations (d) System Converged by 70 Iterations

REFERENCES

[1] Liu, D., and Garimella, S. V., 2005. "Analysis and optimization of the thermal performance of microchannel heat sinks". *Research Publications*(9).

[2] Chen, H. T., Chen, P. L., Horng, J. T., Chang, S. F., Wu, T. Y., and Hung, Y. H., 2006. "Thermal design optimization for strip-fin heat sinks with a ducted air flow". In ITHERM 06, pp. 297–304.

[3] Balagangadhar, D., and Roy, S., 2001. "Design sensitivity analysis and optimization of steady fluid-thermal systems". *Comput. Methods Appl. Mech. Engrg.*(190), pp. 5465–5479.

[4] Borrvall, T., and Petersson, J., 2003. "Topology optimization of fluids in Stokes flow". *International Journal for Numerical Methods in Fluids,* ***41***(1), pp. 77–107.

[5] Gersborg-Hansen, A., Sigmund, O., and Haber, R., 2005. "Topology optimization of channel flow problems". *Structural and Multidisciplinary Optimization*(33), pp. 181–192.

[6] Othmer, C., de Villiers, E., and Weller, H. G., 2007. "Implementation of a continuous adjoint for topology optimization of ducted flows". In 18th AIAA Computational Fluid Dynamics Conference, AIAA, Miami, FL.

[7] Pingen, G., Evgrafov, A., and Maute, K., 2009. "Adjoint parameter sensitivity analysis for the hydrodynamic lattice boltzmann method with applications to design optimization". *Computers and Fluids,* ***38***, pp. 910–923.

[8] Pingen, G., and Meyer, D., 2009. "Design optimization for thermal transport". In Proceedings of the ASME 2009 Fluids Engineering Summer Meeting, August 2-5, 2009, Vail, Colorado, FEDSM2009-78408.

[9] Dede, E. M., 2009. Multiphysics topology optimization of heat transfer and fluid flow systems. Excerpt from the Proceedings of the COMSOL Conference 2009 Boston.

[10] Meyer, D., 2010. "Lattice boltzmann thermal convective topology optimization". Master's thesis, Department of Mechanical and Aerospace Engineering, University of Colorado at Colorado Springs, October.

[11] Gregersen, M. M., Evgrafov, A., and Sorensen, M. P., 2012. "Finite volume based topology optimization of coupled fluid dynamic and thermal conduction systems". In FLOWHEAD Conference on Industrial Design Optimisation for Fluid Flow, Munich, 28-29 March.

[12] Dede, E. M. "Experimental investigation of the thermal performance of a manifold hierarchical microchannel cold plate". In ASME 2011 Pacific Rim Technical Conference and Exhibition on Packaging and Integration of Electronic and Photonic Systems, MEMS and NEMS (InterPACK 2011), Portland, OR.

[13] Dagastine, G. "Numerical simulation-based topology optimization leads to better cooling of electronic components in toyota hybrid vehicles". In Special Advertising Section to IEEE Spectrum: Multiphysics Simulation, June 2012.

[14] Svanberg, K., 1995. "A globally convergent version of MMA without linesearch". In First World Congress of Structural and Multidisciplinary Optimization, G. Rozvany and N. Olhoff, eds., Pergamon, pp. 9–16.

[15] Kreissl, S., Pingen, G., Evgrafov, A., and Maute, K., 2010. "Topology optimization of flexible micro-fluidic devices". *Structural and Multidisciplinary Optimization*(42), pp. 495–516.

[16] Kays, W. M., and Crawford, M. E., 1993. *Convective Heat and Mass Transfer*, 3 ed. McGraw-Hill Series in Mechanical Engineering. McGraw - Hill.

[17] Yu, D., Mei, R., Luo, L.-S., and Shyy, W., 2003. "Viscous flow computations with the method of lattice Boltzmann equation". *Progress in Aerospace Sciences,* ***39***, pp. 329–367.

[18] Luo, L.-S., Krafczyk, M., and Shyy, W., 2010. *Lattice Boltzmann Method for Computational Fluid Dynamics*. Encyclopedia of Aerospace Engineering. Wiley.

[19] Sofonea, V., 2006. "Finite-difference lattice boltzmann approach to pressure-driven microchannel flow with variable temperature". *Euorphysics Letters,* ***76***.

[20] Yan, Y. Y., and Zu, Y. Q., 2008. "Numerical simulation of heat transfer and fluid flow past a rotating isothermal cylinder - a lbm approach". *Internation Journal of Heat and Mass Transfer,* ***51***, pp. 2519–2536.

[21] Kao, P.-H., Chen, Y.-H., and Yang, R.-J., 2008. "Simulations of the macroscopic and mesoscopic natural convection flows within rectangular cavities". *Internation Journal of Heat and Mass Transfer,* ***51***, pp. 3776–3793.

[22] Yoshida, H., and Nagaoka, M., 2010. "Multiple-relaxation-time lattice boltzmann model for the convection and anisotropic diffusion equation". *Journal of Computational Physics*(229), pp. 7774–7795.

[23] Wolf-Gladrow, D. A., 2000. *Lattice-Gas Cellular Automata and Lattice Boltzmann Models: An Introduction*. Lecture Notes in Mathematics. Springer.

[24] Guo, Z., Shi, B., and Zheng, C., 2002. "A coupled lattice BGK model for incompressible thermal flows". *International Journal Numerical Methods Fluids,* ***39(4)***, pp. 325–342.

[25] Spaid, M. A. A., and Phelan, F. R., 1997. "Lattice Boltzmann methods for modelling microscale flow in fibrous porous media". *Physics of Fluids,* ***9***(9), September, pp. 2468–2474.

[26] Pingen, G., Evgrafov, A., and Maute, K. "Towards the topology optimization of fluid-structure interaction problems with immersed boundary techniques". In Proceedings of 2006 NSF DMII Grantees Conference, St. Louis Missouri.

[27] Bendsoe, M., and Sigmund, O., 2003. *Topology Optimization: Theory, Methods and Applications*, 2nd ed. Springer.